BIOCHEMISTRY
including biophysical chemistry & molecular biology

Article

pubs.acs.org/biochemistry

Electrostatic Occlusion and Quaternary Structural Ion Pairing Are Key Determinants of Cu(I)-Mediated Allostery in the Copper-Sensing Operon Repressor (CsoR)

Feng-Ming James Chang, Julia E. Martin, and David P. Giedroc*

Department of Chemistry, Indiana University, Bloomington, Indiana 47405-7102, United States

Supporting Information

ABSTRACT: The copper-sensing operon repressor (CsoR) is an all-α-helical disc-shaped D_2-symmetric homotetramer that forms a 2:1 tetramer/DNA operator complex and represses the expression of copper-resistance genes in a number of bacteria. A previous bioinformatics analysis of CsoR-family repressors distributes Cu(I)-sensing CsoRs in four of seven distinct clades on the basis of global sequence similarity. In this work, we define energetically important determinants of DNA binding in the apo-state ($\Delta\Delta G_{bind}$), and for allosteric negative coupling of Cu(I) binding to DNA binding ($\Delta\Delta G_c$) in a model clade IV CsoR from *Geobacillus thermodenitrificans* (*Gt*) of known structure, by selectively targeting for mutagenesis those charged residues uniquely conserved in clade IV CsoRs. These include a folded N-terminal "tail" and a number of Cu(I)-sensor and clade-specific residues that when mapped onto a model of Cu(I)-bound *Gt* CsoR define a path across one face of the tetramer. We find that Cu(I)-binding prevents formation of the 2:1 "sandwich" complex rather than DNA binding altogether. Folding of the N-terminal tail (residues R18, E22, R74) upon Cu-binding to the periphery of the tetramer inhibits assembly of the 2:1 apoprotein−DNA complex. In contrast, Ala substitution of residues that surround the central "hole" (R65, K101) in the tetramer, as well R48, impact DNA binding. We also identify a quaternary structural ion-pair, E73-K101″, that crosses the tetramer interface, charge-reversal of which restores DNA binding activity, allosteric regulation by Cu(I), and transcriptional derepression by Cu(I) in cells. These findings suggest an "electrostatic occlusion" model, in which basic residues important for DNA binding and/or allostery become sequestered via ion-pairing specifically in the Cu(I)-bound state, and this aids in copper-dependent disassembly of a repression complex.

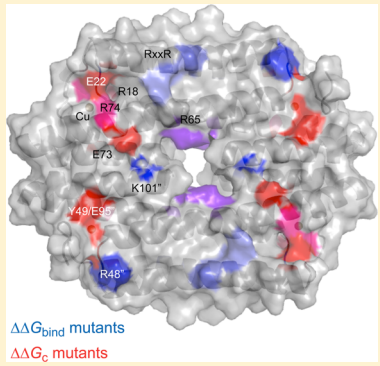

All bacteria encode significant protein-coding machinery that effectively ensures that the concentrations of bioavailable transition metals (Mn to Zn) are tightly regulated relative to one another.[1,2] Although all cells accumulate transition metals, albeit to varying degrees, they have evolved to limit the bioavailability of highly competitive metals, e.g., Cu(I) and Zn(II), by minimizing the "free" or rapidly exchanging pool of these metals.[3,4] This is perhaps best understood for cuprous ion Cu(I), which will predominate under the reducing conditions of the cell cytoplasm.[4] Since many bacteria possess little demonstrable intracellular Cu requirement, this suggests that Cu(I) is simply regarded as bactericidal, and the effects of that toxicity must be mitigated. There is accumulating evidence that elevated cytoplasmic Cu(I) leads to disassembly of solvent-exposed Fe−S clusters, which can have many downstream metabolic effects.[5,6] Since Cu is thought to be concentrated in phagolysosomes in which professional intracellular pathogens, e.g., *Mycobacterium tuberculosis*, are able to survive,[7,8] there remains strong interest in elucidating the molecular details of Cu(I) resistance in bacterial pathogens.

Copper resistance in bacteria is minimally carried out by just three core molecular components:[6] a copper-specific metallosensor that "senses" elevated Cu(I) in the cytoplasm, a Cu(I)-specific membrane transporter that effluxes Cu(I) out of the cytoplasm, e.g., CopA,[9] and in many cases, a dedicated copper chaperone that shepherds Cu(I) to target proteins, e.g., a Cu(I) effluxer or a Cu(I)-specific metallothionein, as found in *Mtb*.[10,11] Cu(I)-specific metallosensors are largely derived from two major structural classes based on *E. coli* CueR[12] and *Mycobacterium tuberculosis* CsoR.[13] Cu(I) coordination to each metallosensor allosterically regulates transcriptional initiation in the case of CueR, and drives transcriptional derepression in the case of CsoR, of genes encoding primary copper resistance proteins. We have developed *Geobacillus thermodenitrificans* (*Gt*) as a model for *Bacillus subtilis* (*Bsu*) and related CsoRs from Gram-positive pathogens due to its favorable relaxation properties, facilitating detailed investigations by NMR spectroscopy[14] and other biophysical techniques.[15] *Gt* CsoR binds to a DNA operator that overlaps the promoter the copper-sensitive operon, encoding *csoR*, *copA*, and the likely chaperone gene, *copZ*.

In previous work, *Gt* CsoR was structurally characterized by X-ray crystallography in the Cu-bound state and by small-angle

Received: February 15, 2015
Revised: March 18, 2015
Published: March 23, 2015

DOI: 10.1021/acs.biochem.5b00154
Biochemistry 2015, 54, 2463−2472

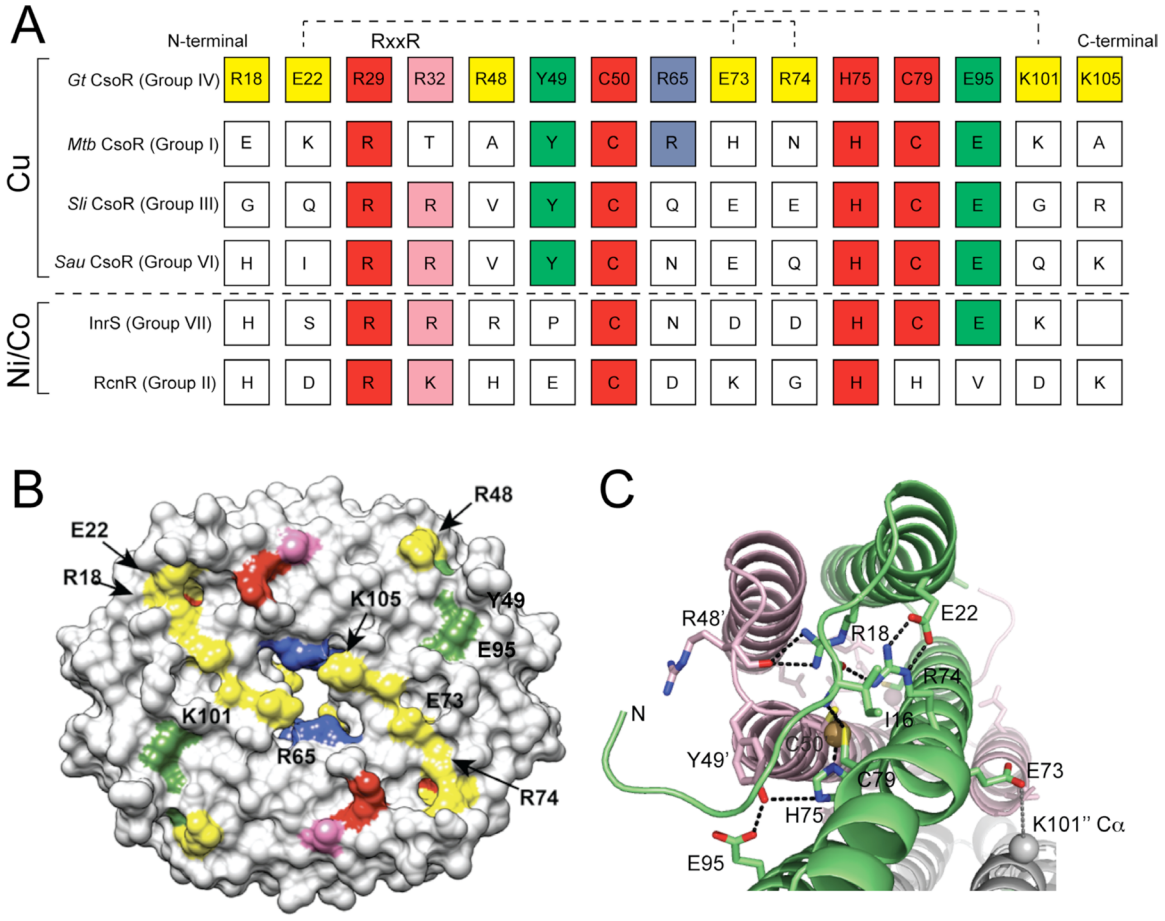

Figure 1. Schematic and surface representation of the conserved clade IV-specific residues. (A) Schematic representation of the residue positions that are conserved across all Cu(I)-sensing CsoRs (shaded red) vs group IV clade-specific residue positions (shaded yellow, *Gt* CsoR residue number indicated). Those residue positions shaded pink are conserved in three of four Cu(I)-containing CsoR groups. Cu(I) second coordination shell ligands are shaded green. R29 and *R*32 in Gt CsoR correspond to the conserved RxxR/K motif identified in previous work of *Sli* and *Mtb* CsoRs shown to be important for DNA binding.[13,22] The dashed lines connect pairs of residues known (E22-R74) or projected (E73-K101) to form an ion pairing interaction in the Cu(I)-bound state of *Gt* CsoR.[15] R65 is shaded blue because in sequences lacking an Arg in this position, an Arg/Lys is often found in the immediately adjacent (+1) residue position. (B) Surface presentation of Cu(I)-*Gt* CsoR crystal structure. Residues are colored based on panel A. (C) Ribbon representation of the Cu(I)-coordination region of the Cu(I)-bund *Gt* CsoR,[15] with selected residues targeted for mutagenesis highlighted in stick.

X-ray scattering, with the rapid time scale protein dynamics studied by $^{1}H-^{15}N$ NMR spectroscopy.[15] *Gt* CsoR adopts the same donut-shaped tetramer structure as other CsoRs including metal-free apo *Streptomyces lividans* CsoR[16] and Cu(I)-bound *M. tuberculosis* CsoR.[13] However, distinct from these previously characterized CsoRs, *Gt* CsoR harbors an N-terminal "tail" that folds over the Cu(I) binding pocket only in the presence of Cu(I). NMR studies reveal that the N-terminal tail is flexible in apo *Gt* CsoR, suggesting that the tail folding could play an important regulatory role in the Cu(I)-mediated allosteric switching mechanism. A phylogenetic analysis previously described reveals that *Gt* CsoR belongs to clade IV CsoR and is representative of this branch of CsoR-family repressors; other distinct clades encode the Ni(II)/Co(II)-specific sensors RcnR[17] and InrS[18] and the persulfide sensor CstR[19] among others.[15,20]

Conserved clade-specific residues in or near the tail region participate in a number of side chain and backbone interactions (Figure 1). These include Arg18 and Glu22 and Arg74 in the α2-helix. Lys101 (Lys96 in *Bsu* CsoR), located at the tetramer interface (between dimers), previously found to be protected from amidination upon DNA binding in a quantitative ratiometric pulsed amidination-mass spectrometry (rPAm-MS) experiment,[21] is also a clade-specific residue (Figure 1A). A candidate salt-bridge between Glu73 and Lys101″ across the *tetramer* interface is also conserved, with the polarity reversed in some CsoR/RcnR family proteins, suggesting that it could be a critical determinant for tetramer stabilization, Cu(I)-mediated allosteric switching, or both (Figure 1B). Moreover, the Lys101 side chain could also be involved in DNA operator binding. Near the center of *Gt* CsoR tetramer, the Arg65 side chain is well modeled and points into the "hole" of the donut (Figure 1B), potentially interacting with C-terminus carboxyl group. The degree these clade-specific and charged residues, outside of a conserved RxxR sequence in the α1 helix (Arg28 and Arg32 in *Gt* CsoR; Figure 1),[13,22] contribute to operator DNA binding and allosteric regulation is generally unclear. In this work, we employ fluorescence anisotropy-based binding experiments coupled with site-directed mutagenesis to elucidate key residues involved in DNA binding and mediation of Cu(I)-induced allosteric switching in *Gt* CsoR *in vitro* and in cells and by inference, other clade IV CsoRs.

DOI: 10.1021/acs.biochem.5b00154
Biochemistry 2015, 54, 2463−2472

MATERIALS AND METHODS

Protein Purification. *Gt* CsoR, expressed from a pET15b plasmid construct in Rosetta BL21(DE3) strain of *Escherichia coli*, was purified as described previously.[15] Uniformly ^{15}N-labeled wild-type and R18A Gt CsoR were expressed essentially as described[14] with transformed *E. coli* grown in M9 salts supplemented with $^{15}NH_4Cl$. Site-directed mutants of CsoR were generated using a standard PCR-based site-directed mutagenesis strategy (Stratagene) and pET15b_Gt CsoR as template. The integrity of all mutant plasmids was confirmed by DNA sequencing with mutant proteins purified as described and mutations verified by mass spectometry.[15] All CsoR mutants were found to possess an approximately tetrameric assembly state by gel filtration chromatography (Table S1, Supporting Information).

Bacterial Copper Induction Experiments. Mutant *Gt csoR* alleles were created by site-directed mutagenesis using pDG1662(*Gt csoR*) vector as a template. Amplified DNA was then transformed into *B. subtilis* strain HB730 (*csoR::spc*) to be integrated at the *amyE* locus.[15] The P_{copZA}-*cat-lacZ* transcriptional fusion was introduced into new strains by SPβ transduction.[23] All mutations were confirmed by sequencing. For β-galactosidase assays, cells from overnight cultures were diluted 1:100 into LB, then subcultured again at mid log phase into prewarmed LB with or without 2 mM $CuSO_4$ to 0.1 OD_{600} and aerated at 37 °C for 3 h. β-Galactosidase activity was measured at room temperature.

Copper Binding Assays. Bathocuproine disulfonate (BCS) or bicinchoninic acid (BCA) were used for Cu(I) binding affinity determination of *Gt* CsoR by titration of apoprotein into a chelator−copper complex.[24] Apoproteins were buffer exchanged into degassed buffer A (25 mM HEPES, pH 7.0, 200 mM NaCl) in an anaerobic chamber. The Cu(I) stock was prepared by taking the supernatant following anaerobic dissolution of solid CuCl into fully degassed buffer A (25 mM HEPES, pH 7.0, 200 mM NaCl). The concentration of Cu(I) stock was determined by atomic absorption spectroscopy (PerkinElmer AAS-400) with a typical stock concentration of ∼10 mM. A concentrated stock solution of fully reduced apo-CsoR was titrated into a solution containing 40−60 μM Cu(I) and 100−150 μM BCS or 100−150 μM BCA; under these conditions, all of the Cu(I) is bound as a Cu(I):BCS_2 or Cu(I):BCA_2 complex, respectively, before addition of apo CsoR. The optical spectra of BCA or BCS were recorded from 200 to 900 nm, and corrected spectra were obtained by subtracting the apo CsoR spectrum from each Cu(I)-addition spectrum and then correcting for dilution. The A_{483} value was used to determine the concentration of $Cu(BCS)_2$ complex using a molar extinction coefficient of 13 000 M^{-1} cm^{-1}. The A_{562} value was used to determine the concentration of the Cu(I)−BCA_2 complex with an extinction coefficient of 7900 M^{-1} cm^{-1}. Data were fitted to the appropriate competition model using Dynafit.[25]

NMR Experiments. Both apo and Cu(I) CsoR (wild-type and R18A) were prepared at ∼1.0 mM protomer in Buffer N (10 mM MES, 120 mM NaCl, 5 mM TCEP, 5 mM EDTA, 20 mM arginine, 20 mM glutamate, pH 6.0). All NMR experiments were performed at 800 MHz Varian (Agilent) DDR spectrometer at 318 K in the METACyt Biomolecular NMR Laboratory at Indiana University. All ^{1}H−^{15}N HSQC experiments were acquired as TROSY spectra given the large size of this tetrameric assembly (47.7 kDa).[14]

Fluorescence Anisotropy Experiments. A 41 bp 3′-fluorescein-labeled operator duplex DNA was derived from the operator-promoter region of *cso* operon (5′-GTTGTAACTAT-ATACCCCCTTCGGGTATAAT-GTATATAGAC-3′). The double-stranded DNA was synthesized, purified, and annealed from component single strands as described previously.[15] Fluorescence anisotropy measurements were performed by using a Biotek Synergy H1 Hybrid Multimode microplate reader with a λ_{ex} of 487 nm. A typical experiment was conducted in triplicate in a 96-well format with 10 nM duplex DNA operator in 20 mM sodium phosphate, 130 mM NaCl, pH 6.5 at 25.0 °C, and various concentrations of CsoR. Normalized r values (ranging from 0 to 1) represent fractional saturation of the DNA and were calculated from the ratio $(r_{obs} - r_{DNA})/(r_{max} - r_{DNA})$ where r_{max} is the maximum anisotropy obtained at saturating protein concentrations and r_{DNA} is the anisotropy of the free DNA. The resultant data were subjected to an weighted nonlinear least-squares fit to a two-tetramer stepwise binding model (defined by K_1 and K_2) to A and B sites on the operator (see Figure 2) using Dynafit[25] and assuming a linear relationship between r_{obs} and fractional saturation of the DNA as verified previously.[26] Since intrinsic site binding affinities defined by k_A and k_B can not be defined by these data, k_A and k_B are constrained to be equal, $k_A = k_B = K$ where $K_1 = A_1 = 2*K$ and $K_2 = (K/2)\omega^*$, where ω^* is measure of the degree to which binding of the first tetramer enhances ($\omega^* > 1$) or inhibits ($\omega^* < 1$) the binding of the second tetramer to the

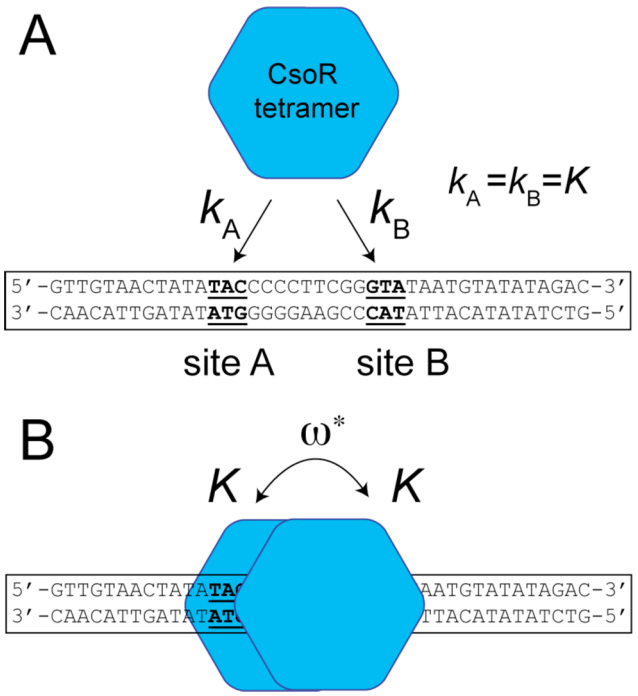

Figure 2. Schematic diagram of a simplified 2:1 CsoR DNA binding model used here. (A) The first CsoR tetramer binding event to operator DNA. The base pairs which are predicted as a B- to A-form DNA junction are shown in bold, e.g., TAlC. k_A and k_B are intrinsic site binding affinities for sites A and B, respectively. Since k_A and k_B cannot be uniquely defined in these experiments, we assume here that $k_A = k_B = K$. (B) Two CsoR tetramers bound to DNA, with the intrinsic binding affinity K linked by the parameter ω^*. ω^* is a measure of the degree to which binding of the second tetramer binds with higher ($\omega^* > 1$) or lower ($\omega^* < 1$) affinity relative to the first (see text for details).

DOI: 10.1021/acs.biochem.5b00154
Biochemistry 2015, 54, 2463−2472

Table 1. Operator DNA Binding Properties for *Gt* CsoRs[a]

Gt CsoR		DNA binding affinity		ΔG_c (kcal/mol)	r_0	r_∞
		ω^* (= $2K_2/K_1$)[b]	A_2 ($\times 10^{13}$ M^{-2})[c]			
WT	apo	7.7 (±0.9)	6.9 (±1.6)	>3.3 (±0.2)	105	129
	Cu(I)	n.d.	<0.027 (±0.004)		104.8	128.8
Y49F/E95Q	apo	15 (±2.2)	14 (±2.0)	1.8 (±0.3)	100.7	124.7
	Cu(I)	0.8 (±0.2)	0.61 (±0.14)		96.8	120.8
R18A	apo	2.6 (±0.5)	2.4 (±0.4)	1.2 (±0.4)	96	120
	Cu(I)	0.43 (±0.16)	0.32 (±0.12)		115	139
E22A	apo	16 (±2.3)	14.0 (±2.1)	1.3 (±0.2)	104.3	128.3
	Cu(I)	2.0 (±0.3)	1.5 (±0.2)		111	135
R74A	apo	1.1 (±0.2)	1.0 (±0.2)	0.6 (±0.4)	106.6	130.6
	Cu(I)	0.47 (±0.16)	0.35 (±0.12)		103.2	127.2
R65A[d]	apo	1.1 (±0.2)	1.0 (±0.2)	1.7 (±1.2)	100.3	124.3
	Cu(I)	0.08 (±0.10)	0.06 (±0.08)		116.6	140.6
R48A	apo	n.d.[e]	<0.018 (±0.003)	n.d.	103.5	127.5
	Cu(I)	n.d.	<0.006 (±0.002)		100.5	124.5
K101E	apo	n.d.	<0.009 (±0.003)	n.d.	97.5	121.5
	Cu(I)	n.d.	<0.004 (±0.003)		91.1	115.1
E73K/K101E	apo	2.6 (±0.3)	2.3 (±0.3)	>3.0 (±0.3)	101.8	125.8
	Cu(I)	n.d.	<0.015 (±0.004)		99.5	123.5

[a]20 mM NaP_i, pH 6.5, 130 mM NaCl, 25.0 °C, 10 nM DNA duplex. [b]ω^*, measure of the degree to which the second tetramer binds more tighly that the first, defined as $2K_2/K_1$. K_1 for wild-type (WT) apo and Cu(I)-CsoR were determined as 6.0×10^6 M^{-1} and 5.5×10^6 M^{-1}, respectively. These two values were constrained for all mutants and K_2 determined by nonlinear least-squares fitting in Dynafit (see Materials and Methods).[25] [c]A_2 is defined as $K_1 \cdot K_2/2$. [d]Data reported previously,[15] and shown here for reference. [e]n.d., could not be determined, defined by the following lower limits $K_2 < 10^4$ M^{-1}, $A_2 < 10^{10}$ M^{-2} under these solution conditions. All mutants are approximately tetrameric as revealed by gel filtration chromatography (Table S1).

DNA. Note that ω^* is not a true cooperativity parameter, but an apparent value derived from an inability to resolve k_A from k_B. The macroscopic DNA binding constant A_2, is determined from $A_2 = K_1K_2 = K^2\omega^*$ (see Table 1). Allosteric coupling free energies, ΔG_c, are calculated as $\Delta G_c = -RT \ln(A_2^{Cu}/A_2^{apo})$, with A_2^{Cu} and A_2^{apo} corresponding to macroscopic DNA binding constants of 2:1 Cu(I)-bound and apo-CsoR:DNA complexes, respectively. We note that K_2 and thus A_2 were obtained for all mutants by assuming that K_1 is identical to that of wild-type CsoR, in the absence and presence of bound Cu(I). This is justified by the strong anticorrelative nature of K_1 and K_2, which prevents resolution of unique values for K_1 and K_2, particularly in the case of weak binding. Since A_2 is given by K_1K_2, and $\Delta\Delta G_c$ and $\Delta\Delta G_{bind}$ are obtained from A_2 values (*vide infra*), this simplifying assumption provides a straightforward approach to compare mutant CsoRs.

RESULTS AND DISCUSSION

Copper Binding Affinity of Gt CsoR. The copper(I) binding properties of *Gt* CsoR were examined using a chelator competition assay.[24] Bathocuproine disulfonate (BCS) and bicinchoninic acid (BCA) are small molecule chelators that bind to Cu(I) with high affinity and form 1:2 complexes with Cu(I), log $\beta 2$ = 19.8 for Cu(I):$(BCS)_2$ and log $\beta 2$ = 17.2 for Cu(I):$(BCA)_2$,[27] and were used to estimate the Cu(I) binding affinity of *Gt* CsoR. A BCS competition assay was initially performed by titrating apoprotein into Cu(I):$(BCS)_2$ which resulted in protein precipitation. A BCA competition assay was then carried out by titrating apo-CsoR into Cu(I)/$(BCA)_2$ at two concentrations and a global fit of two binding curves performed using Dynafit with 1:1 (Cu:protomer) binding model (Figure S1, Supporting Information).[28] This yields a cuprous ion binding affinity of 4.1 (±0.8) $\times 10^{14}$ M^{-1} at 25.0 °C, pH 7.0, 0.2 M NaCl. Although ~10^4-fold weaker than K_{Cu} measured for other mesophilic CsoRs, including *B. subtilis* CsoR, under similar solution conditions,[28−30] *Gt* CsoR remains capable of functioning as a Cu-regulated repressor in *B. subtilis* grown at 37 °C.[15] This K_{Cu} determined at 25 °C may reflect a significant temperature dependence of K_{Cu} since this *Geobacillus* strain grows optimally at 65 °C.

DNA Binding and Functional Properties of Wild-Type and Clade IV Mutant Gt CsoRs. We previously investigated the Cu(I)-dependent regulation of operator DNA binding equilibria of wild-type *Gt* CsoR *in vitro* using a fluorescence anisotropy-based DNA binding assay.[15] Here, a fluorescein-labeled 41-bp dsDNA harboring the minimal pseudopalindromic TA|CCCCCTTCGGG|TA motif[29] was added to each well on a 96-well plate at 10 nM DNA to which increasing concentrations of CsoR was added. All binding data were fitted with a 2:1 tetramer/DNA binding model as described in Materials and Methods.[25] Previous experiments with *B. subtilis* CsoR and *S. lividans* CsoR[22] reveal a 2:1 tetramer/DNA binding stoichiometry, a finding fully consistent with a preliminary titration with *Gt* CsoR as measured by isothermal titration calorimetry (ITC) (Figure S2, Supporting Information). Interestingly, performing the same experiment with Cu(I)-bound *Gt* CsoR yields no detectable heat (Figure S2) as previously shown from *S. lividans* CsoR,[22] consistent with either very weak binding and/or a substantially distinct binding mode in the allosterically inhibited state.

Binding Model. We used the following approach to analyze the fluorescence anisotropy-based binding isotherms. We first carried out an optimized two parameter fit, solving for K_1 and K_2, where fitted $K_1 = A_1 = (k_A + k_B)$ and $K_2 = \mathrm{sqrt}(k_Ak_B)$ where A_1 is the macroscopic affinity of the 1:1 complex with CsoR bound to either site A or site B (see Figure 2) defined by intrinsic site binding affinities k_A and k_B, respectively. A_2 is the overall macroscopic constant for formation of the 2:1 complex

DOI: 10.1021/acs.biochem.5b00154
Biochemistry 2015, 54, 2463−2472

from free tetramer and DNA, $A_2 = (K_1/2)K_2$. Since we cannot confidently measure k_A and k_B independently of one another due to a lack of individual site-binding curves, we made the further simplification in this work that $k_A = k_B = K$ and that $A_1 = 2K$ and $A_2 = K^2\omega^*$, where ω^* is a measure of the degree to which binding of the first CsoR tetramer stimulates ($\omega^* > 1$) or inhibits ($\omega^* < 1$) the binding of the second tetramer to the DNA and therefore provides a descriptor of the degree to which K_1 differs from K_2 (Figure 2). We used the average value of the unconstrained fits for K_1 for wild-type apo- or Cu(I)-bound CsoRs as a fixed parameter and nonlinear least-squares fit to obtain the value of K_2, from which ω^* is extracted arithmetically, for all mutants. K_1 was found to be 6.0×10^6 M^{-1} for apo-CsoR and 5.5×10^6 M^{-1} for Cu(I)-CsoR, the latter obtained by fitting to a 1:1 binding model since Θ never goes beyond 0.5, thus suggestive of a 1:1 complex for Cu(I)-bound CsoR (Figure 3A). These values are identical to those reported previously using a similar binding model.[15] The optimized values of ω^* and A_2 obtained in this way are compiled in Table 1 for the apo- and Cu(I)-bound forms of all wild-type and mutant CsoRs, as is the allosteric coupling energy ΔG_c.

ω^* for the binding of apo wild-type CsoR to DNA is 7.7 ($\pm$0.9) (Table 1). Species fractions of 1:1 and 2:1 tetramer/DNA complexes are plotted as a function of total [apo-CsoR] calculated from the binding parameters (Figure S3B) reveal that when saturation of binding is reached ($\Theta = 1$); the 2:1 CsoR-DNA complex (Figure S3B, red dashed curve) is the dominant species in solution. These data reveal that apo-CsoR binds to the DNA in such a way that the second tetramer binds with slightly higher affinity than the first, leading to a 2:1 complex, with concomitant disappearance of the 1:1 complex (see simulations, Figure S3B,D). In the presence of Cu(I), the affinity of a second tetramer for the DNA operator is most significantly attenuated since the fractional saturation (Θ) does not exceed 0.5 (Figure S3C). A similar finding was reported for *B. subtilis* CsoR.[26] The overall binding affinity A_2 for apo and Cu(I)-CsoR can be calculated as 6.9 ($\pm$1.6) $\times 10^{13}$ M^{-2} (A_2^{apo}) and $\leq$2.7 ($\pm$0.4) 10^{12} M^{-2} (A_2^{Cu}), revealing a $\geq$ 20-fold reduction in overall DNA binding affinity (Table 1). This suggests that Cu(I) inhibits assembly of the apo-CsoR-DNA complex largely via destabilization of a second tetramer binding event. As discussed previously, the coupling free energy ΔG_c is a measure of the degree of allosteric regulation as relative fractions of the 2:1 species with that of free DNA and is determined by $\Delta G_c = -RT \ln(A_2^{Cu}/A_2^{apo})$. The allosteric coupling free energy of wild-type CsoR ($\Delta G_{c,wt}$) is calculated as $\geq$3.3 ($\pm$0.2) kcal/mol (Table 1), which is a lower limit due to inability to determine K_2^{Cu}. This corresponds to strong negative allosteric regulation of DNA operator binding by Cu(I).

Y49F/E95Q Gt CsoR. Previous studies on *Bsu* CsoR and *Mtb* CsoR reveal that conserved residues Tyr49 and Glu95 in the Cu(I) chelate region maintain wild-type like Cu(I)-dependent allosteric switching (Figure 1C).[26,28] Here, we investigated the effect of substitutions of these two residues, as a single- (E95A) or double-substitution mutant (Y49F/E49Q) *Gt* CsoRs. β-galactosidase activities were measured in the presence and absence of 2 mM Cu added in *csoR*-null strains of *B. subtilis* harboring a *Gt copZA* operator-promoter region driving expression of the *lacZ* gene, complemented with either wild-type, E95A or Y49F/E95Q CsoRs (Figure 4A). Although both E95A and Y49F/E95Q CsoRs repress *lacZ* expression to the same degree as wild-type CsoR in the absence of Cu(I), each is

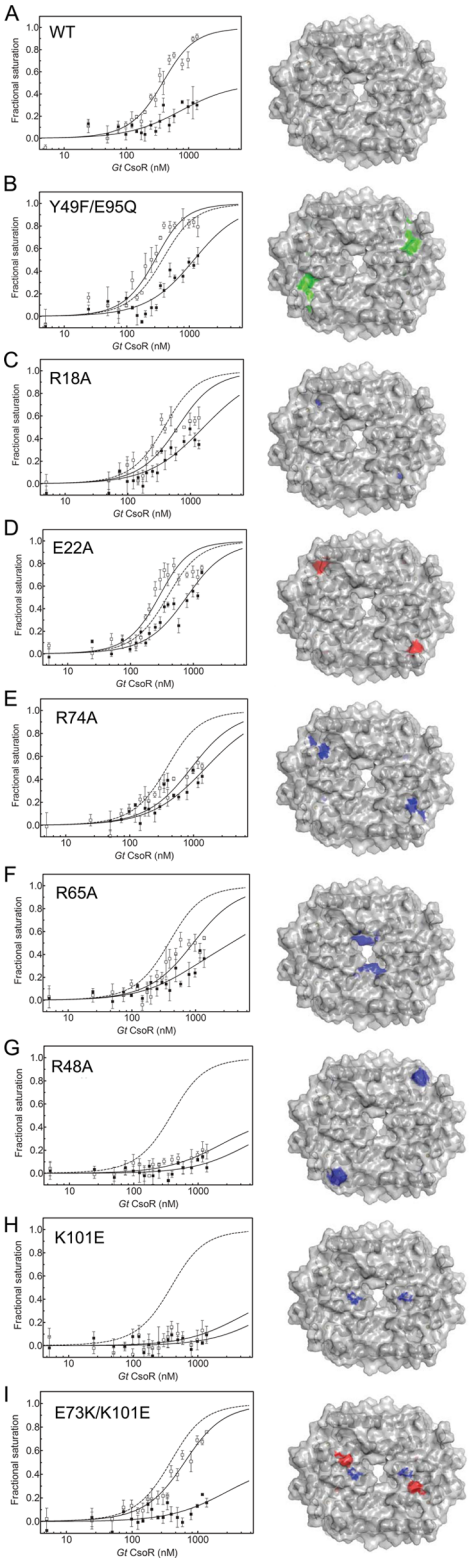

Figure 3. Normalized fluorescence-anisotropy-based triplicate DNA binding isotherms for wild-type and mutant *Gt* CsoRs acquired in the absence (open squares) and presence (closed squares) of 2 mM Cu, with continuous lines through the data the results of a weighted, nonlinear least-squares fit to a two-tetramer, cooperative DNA binding model with the fitted parameters compiled in Table 1. The dashed isotherm shown in panels B–I, left, represents the best-fit DNA binding curve for apo-wild-type CsoR from panel A. The physical locations of each residue targeted for mutagenesis is shown on a space-filling model of Cu(I)-*Gt* CsoR are shown to the right in each panel,

DOI: 10.1021/acs.biochem.5b00154
Biochemistry 2015, 54, 2463–2472

Figure 3. continued

shaded green, blue, and red for second-shell, basic and acidic residues, respectively. (A) wild-type (WT), reproduced from ref 15; (B) Y49F/E95Q; (C) R18A; (D) E22A; (E) R74A; (F) R65A;[15] (G) R48A; (H) K101E, (I) E73K/K101E *Gt* CsoRs.

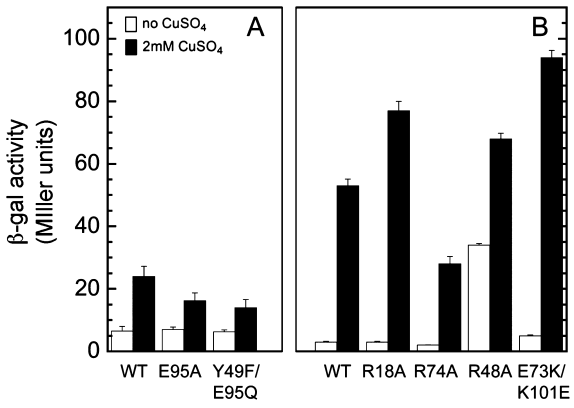

Figure 4. *β*-galactosidase activities of (A) wild-type (WT) *Gt* CsoR, E95A *Gt* CsoR, and Y49F/E95Q *Gt* CsoRs or (B) wild-type, R18A, R74A, R48A, and E73K/K101E *Gt* CsoRs complemented *B. subtilis csoR*-null strain harboring *cop*ZA promoter-*lacZ* fusion as reporter analyzed in LB medium with or without addition of 2 mM $CuSO_4$.[15]

modestly attenuated in Cu(I)-dependent derepression; this suggests a measurable impact of this "second-coordination shell" network on allosteric negative regulation of O/P binding by Cu(I).

To test this, we carried out fluorescence-based DNA binding with Y49F/E95Q CsoR (Figure 3B) with the binding parameters compiled in Table 1. The simulated species fractions for apo Y49F/E95Q CsoR (Figure S4B) and Cu(I)-loaded Y49F/E95Q CsoR (Figure S4C) reveal that apo Y49F/E95Q CsoR has species fraction distribution of 1:1 and 2:1 complexes that is similar to that of apo wild-type CsoR consistent with a wild-type-like DNA binding affinity *in vitro* (Figure S4B; Table 1) and in cells (Figure 4A). In contrast, Cu(I)-loaded Y49F/E95Q CsoR binds DNA more tightly than Cu(I)-loaded wild-type CsoR, consistent with an increased population of 2:1 complex forming at high [CsoR] (Figure S4C, red dashed curve). The A_2^{apo} (1.4 (±0.2) × 10^{14} M^{-2}) and A_2^{Cu} (6.1 (±1.4) × 10^{12} M^{-2}) reveals a coupling free energy of 1.8 (±0.3) kcal/mol, which is smaller than wild-type CsoR (Table 1). These data taken collectively reveal that this second coordination shell contributes to the magnitude of allosteric coupling in clade IV CsoRs, but substitutions do not eliminate coupling altogether either *in vitro* or in cells; quantitatively similar findings characterize a clade I[15] *Mtb* CsoR.[28] This finding is similar to the functional results reported for a D91A mutant in *Listeria monocytogenes* CsoR, another clade IV CsoR.[31]

A comparison of the $^1H-^{15}N$ TROSY spectra of E95A and Y49F/E95Q CsoR in the Cu(I)-bound states are consistent with these functional findings (Figure S5C). These spectra are highly similar to one another, revealing that Cu(I)-binding to these mutants do indeed switch the conformation from an apo-like to a Cu(I)-like state.[14] However, there are some subtle differences, most notably in the crosspeak position of the NH of Ile16, which is a sensitive indicator of folding of the N-terminal tail over the Cu(I) binding site (Figure 1C).[15] This is also true for R18A CsoR, discussed further below. This suggests small changes in structure and/or dynamics result from perturbation of this network, which collectively lead to a decrease in ΔG_c.

R18A Gt CsoR. Our crystal structure of *Gt* CsoR[15] reveals that the side chain of R18 is completely buried and hydrogen bonds to the backbone carbonyl oxygen atom of R48 to make a critical interaction upon Cu(I)-induced folding of the N-terminal region (see Figure 1C). We reasoned that ordering of the N-terminal tail could contribute to Cu(I)-mediated allosteric switching, thereby distinguishing clade IV CsoRs from others, and tested this with an R18A mutant. On the one hand, an Ala substitution might perturb folding and reduce the magnitude of ΔG_c. On the other hand, the positively charged Arg18 side chain could directly interact with DNA in the apo-state, with Cu(I) binding leading to a sequestration of the side chain and loss of a key DNA-binding determinant. In this case, an alanine substitution would result in a large decrease in the DNA binding affinity of apo-CsoR. A quantitative analysis of the fluorescence-anisotropy-based binding isotherms (Figure 3C) obtained in the apo-state vs the Cu(I)-bound state for R18A CsoR reveals only a small (~3-fold) diminution in apo-state DNA binding affinity, but increased affinity for the Cu(I)-bound state, revealing defective allosteric coupling of Cu(I) and DNA binding, or ΔG_c of 1.2 (±0.4) kcal mol^{-1} (Table 1).

To facilitate a comparison of this and other mutant CsoRs while permitting quantification of the relative impact of a particular CsoR substitution on apo-state DNA binding affinity vs allosteric coupling of Cu(I) and DNA binding, we introduce two additional terms. $\Delta\Delta G_{bind}^{apo}$ is defined as difference in binding free energies of the mutant relative to the wild-type protein, $\Delta\Delta G_{bind} = \Delta G_{bind}^{mutant} - \Delta G_{bind}^{WT} = -RT \ln(A_2^{mutant,apo}/A_2^{WT,apo})$ (see Figure 5, yellow bars). A large value of $\Delta\Delta G_{bind}$ reveals that the substituted residue plays an energetically significant role in maintaining DNA binding affinity. Likewise, $\Delta\Delta G_c^{mutant}$ measures the impact of a mutation on the degree of Cu(I) capable of driving Cu-mediated disassembly, which is defined as $\Delta G_c^{WT} - \Delta G_c^{mutant}$.

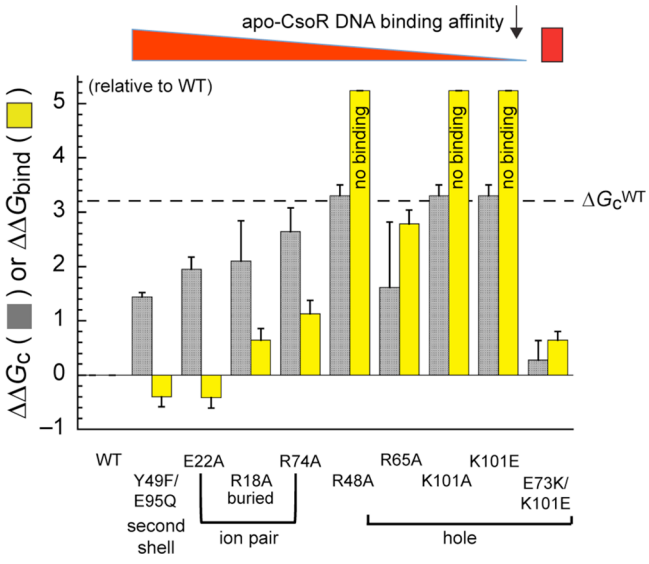

Figure 5. Graphical summary of the impact of individual or pairs of mutations on controlling the magnitude of Cu(I)-dependent allostery ($\Delta\Delta G_c$, gray bars) or DNA-binding in the apo-state ($\Delta\Delta G_{bind}$, yellow bars).

DOI: 10.1021/acs.biochem.5b00154
Biochemistry 2015, 54, 2463−2472

A large value of $\Delta\Delta G_c^{mutant}$ corresponds to significant effect of that mutation on allosteric negative regulation of DNA binding (see Figure 5, gray bars). $\Delta\Delta G_{bind}^{R18A}$ is 0.6 (±0.2) kcal mol^{-1}, while $\Delta\Delta G_c^{R18A}$ is ≥2.1 kcal mol^{-1} (Table 1). Since $\Delta\Delta G_c^{R18A}$ is larger than $\Delta\Delta G_{bind}^{R18A}$, this indicates that the Arg18 side chain has a more significant defect in allosteric coupling than in mediating a direct interaction with DNA in the apo state. Thus, like Y49F/E95Q CsoR, R18A CsoR is largely an allosteric mutant. *In vivo* analysis of R18A CsoR reveals robust repression and Cu(I)-induced derepression, revealing that this relatively modest effect on Cu(I)-induced allostery is not readily detected in cells (Figure 4B).

A comparison of the ^{1}H−^{15}N TROSY spectra of apo (Figure S5A) and Cu(I)-loaded (Figure S5B) wild-type and R18A *Gt* CsoRs reveal the R18A mutation does not perturb the global structure in apo-state to any significant degree, consistent with the fact that the N-terminus to residue 20 is unstructured and quite flexible on the picosecond-nanosecond time scale in the apo-state.[14,15] In contrast, the R18A substitution does have a measurable influence on the overall structure of Cu(I)-bound protein since most cross peaks are shifted or perturbed relative to the wild-type Cu(I)-CsoR (Figure S4B). The Ile16 crosspeak, while nearby the same crosspeak in wild-type CsoR is far less intense, suggesting decreased ordering of the N-terminal tail and/or increased solvent exchange on conformational dynamics in this region. Thus, these NMR spectra provide a possible structural origin for the small allosteric defect in the R18A CsoR and suggest that N-terminal tail folding is energetically tied to the magnitude of ΔG_c in clade IV CsoRs which is conserved as Arg/Lys (Figure S6).[15]

E22A and R74A Gt CsoRs. Inspection of our structure[15] reveals that the Arg74 side chain interacts with Pro17 and the Arg18 backbone carbonyl group, while forming a ion-pairing interaction with Glu22, the second residue in the α1 helix (Figure 1C). Like Arg18, both Glu22 and Arg74 are clade IV-specific residues (Figure 1A) and thus may be involved in Cu(I)-mediated N-terminal tail ordering; in addition, Arg74 may also interact with the DNA in the apo-state. Single alanine substitution mutants of Glu22 and Arg74 were therefore prepared and DNA binding properties were investigated by fluorescence anisotropy as described above. Apo-E22A CsoR binds DNA with an ≈2-fold overall increased affinity relative to wild-type CsoR (Figure 3D; Table 1), visualized by the species fractions simulations of 1:1 and 2:1 complexes (Figure S7B,D). However, in the presence of Cu(I), E22A CsoR exhibits weaker negative regulation of DNA binding, with ΔG_c of 1.3 (±0.2) kcal mol^{-1} or just 30% that of wild-type CsoR (Table 1).

In contrast to the R18A mutant, apo R74A *Gt* CsoR has significantly *reduced* DNA binding affinity (~6-fold), with much of the enhanced affinity of the second tetramer lost in this mutant as well [ω^* = 1.1 (±0.2)] (Table 1; Figure S8). However, like E22A CsoR, ΔG_c of R74A is significantly smaller than wild-type CsoR (Table 1), visualized in the species fractionation analysis (Figure S8). Thus, R74A CsoR is a "mixed" mutant; however, since $\Delta\Delta G_c > \Delta\Delta G_{bind}^{apo}$, these data taken collectively reveal that the Glu22-Arg74 ion pairing interaction, uniquely conserved in clade IV CsoRs (Figure 1), enhances conversion of apo CsoR from a high affinity to low affinity DNA-binding repressor in the presence of Cu(I). Relative to Arg18, Arg74 also plays an energetically significant role in DNA binding since $\Delta\Delta G_{bind}^{apo}$ is not zero, a finding consistent with the *higher* affinity of E22A CsoR, which would eliminate an electrostatically repulsive interaction with the DNA in the same region of the complex. Characterization of R74A CsoR in cells reveals that, like the second coordination shell mutant Y49F/E95Q CsoR, Cu(I)-induction of *lacZ* expression is attenuated relative to wild-type CsoR (Figure 4B).

The reduced apo-state DNA binding affinity observed for R74A CsoR is identical within experimental error to that of R65A CsoR previously characterized, with the binding isotherms (Figure 3F) and binding parameters (Table 1) recapitulated here for comparison.[15] However, unlike R74A CsoR, R65A CsoR retains significantly higher ΔG_c (1.7 vs 0.6 kcal mol^{-1}) as required by the ≈5-fold lower affinity of the Cu(I)-bound state for the operator relative to R74A CsoR. Thus, while R65A CsoR is also a "mixed" mutant, $\Delta\Delta G_c \approx \Delta\Delta G_{bind}^{apo}$ suggesting that Arg65 may well be an important determinant for DNA binding, consistent with its position near the "hole" of the tetramer, along with K101 and K105, reported earlier[15] and near the conserved RxxR motif (Arg29 and Arg32 in *Gt* CsoR; Figure 1A) characterized in *Sli* CsoR.[22] Since most CsoR-family repressors harbor an Arg/Lys residue in the position corresponding either to Arg65 or in the immediately adjacent residue position (Figure 1A), this region of the α2 helix may define a conserved DNA binding region.[15] Indeed, Arg65 corresponds to Lys60 in the related clade IV *B. subtilis* CsoR, whose chemical reactivity is attenuated in the DNA-bound complex.[21]

R48A Gt CsoR. Arg48 is a clade IV-specific residue that is "off" the imaginary "clade" line that crosses one face of the tetramer from "northwest to southeast" in the orientation shown (Figure 1B). However, as pointed out above, the backbone carbonyl oxygen of Arg48′ in the opposite protomer accepts the hydrogen bond from the Arg18 side chain, and thus emerges from the opposite side of the tetramer, near the second shell residue Tyr49 and Cu(I)-ligand Cys50 (Figure 1C). We therefore characterized R48A CsoR to assess the impact of this residue on CsoR function. Strikingly this mutant is essentially inactive in DNA binding, with little residual Cu(I)-dependent negative regulation observable (Figure 3G; Table 1). Consistent with these physical parameters, R48A CsoR is a weak repressor in cells, with unregulated *lacZ* expression increased 10-fold relative wild-type CsoR, that is only modestly induced in the presence of Cu(I) (Figure 4B).

Evidence for a Functionally Critical K101-E73″ Ion Pairing Interaction Across the Tetramer Interface. Inspection of our structure reveals that the side chain of Lys101, although not visible in the structure, could be positioned to form an ion pairing interaction with Glu73″, across the tetramer interface (Figure 1C); furthermore, inspection of other non-Cu(I)-sensing CsoRs suggests that may be a generally conserved feature of all CsoR-family repressors, with this putative interaction charge-reversed in the Ni/Co-sensor RcnR (Figure 1A). Previous studies establish that a K101A mutant is inactive in DNA binding in the apo-state[15] and that the reactivity of the analogous residue in the closely related *Bsu* CsoR (Lys96) toward a small-molecule amidinating reagent is protected in *both* the Cu-bound state and the DNA-bound state relative to apo-CsoR.[21] We therefore characterized K101E CsoR and the corresponding charge reversed double mutant, E73K/K101E CsoR. As anticipated from the K101A mutant,[15] K101E CsoR is essentially inactive in DNA binding, with virtually no effect of Cu(I) binding on these equilibria. In striking contrast, the charge reversal mutant is characterized by DNA binding properties in the apo- and Cu(I)-bound states (Figure 3I) that

DOI: 10.1021/acs.biochem.5b00154
Biochemistry 2015, 54, 2463−2472

are nearly indistinguishable from that of wild-type CsoR (Table 1); furthermore, this mutant is fully active in cells (Figure 4B).

CONCLUSIONS

In this work, site-directed mutagenesis and quantitative DNA binding assays have been used to investigate Cu(I)-mediated allosteric regulation in a structurally characterized Cu(I)-sensing CsoR from *Geobacilllus thermodenitrificans* as a model for other closely related clade IV-specific CsoRs.[15,32] In previous work, we established global features of Cu(I)-dependent conformational switching in *Gt* CsoR, which involves folding of the N-terminal tail region over the Cu(I)-binding site, and a change in the hydrodynamic properties of the molecule to a more compact state, in which one dimer within this D_2-symeetric homotetramer appears to reorient relative to the other.[15] These is, as yet, no high resolution structure of a DNA-bound CsoR-family repressor in either a 1:1[33] or 2:1[22] complex; as a result, molecular insights remain generally lacking as to how these conformational changes lead to Cu(I)-dependent destabilization or disassembly of this protein−DNA complex.

Given that this conformational change may well be subtle,[15] we reasoned that positively charged residues on the surface of one face of the CsoR tetramer might form energetically significant contacts with the DNA in the apo-state, which then become "sequestered" or "occluded" via ion pairing in the Cu(I)-bound state, reducing protein−DNA complex stability. Such residues would be distinguished from the RxxR motif in the α1 helix found in virtually all CsoR-family members, which although previously shown to be important for DNA binding in a number of CsoRs,[13,22] are exposed to solvent in both the apo- and Cu(I)-bound states and thus can not be Cu(I)-regulatory for DNA binding. The clade IV-specific Arg48 in *Gt* CsoR studied here may well be in this category as well, and this is discussed further below. Three known or inferred ion pairing interactions can be identified from inspection of our tetramer structure: Glu22-Arg74, Arg65-α-COO^-, and Glu73-Lys101″, the latter of which reaches across the tetramer interface (Figure 1B).

The impact of a number of single and double mutations characterized here on driving Cu(I)-dependent allostery ($\Delta\Delta G_c$) vs maintaining wild-type-like assembly of the 2:1 apo-CsoR/DNA complex ($\Delta\Delta G_{bind}$) are summarized in Figure 5 in graphical form and in Figure 6 schematically. This quantitative analysis provides support for an electrostatic sequestration for Arg65 and Lys101, and to a lesser degree Arg74, and not at all for Arg18, as Ala substitutions of each of these mutants weakens the affinity of the apo-state to an extent that increases as one moves from the periphery of the tetramer to the "hole" as evidenced in the approximate rank order of $\Delta\Delta G_{bind}$ from Arg18 to Arg74 to Arg65 to Lys101 (Figure 5). In contrast, $\Delta\Delta G_c$ is far greater than $\Delta\Delta G_{bind}$ at the periphery, e.g., in folding the N-terminal tail region, although as one moves closer to the middle of the molecule, this dichotomy of function can not be separated since the low DNA binding affinity in the apo-state will necessarily depress the magnitude of ΔG_c, due to a lower limit on the DNA binding affinity that is measurable with this assay in the presence of absence of Cu(I) (Figure 5). Since Arg74, Arg65, and Lys101 are clearly key DNA binding determinants, Cu(I)-dependent allostery may well involve shielding these residues from base-specific or nonspecific electrostatic interactions by ion pairing that

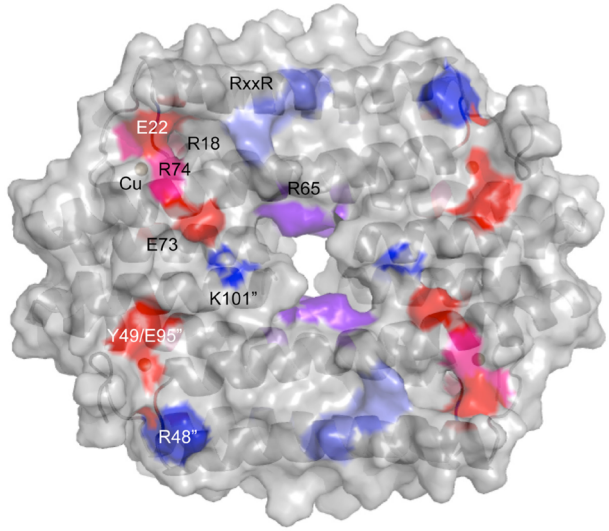

Figure 6. Schematic summary of the functional role played by each residue in *Gt* CsoR targeted for mutagenesis in this and previous work[15] (see text for details). Residues important for facilitating the Cu(I)-specific allosteric response are shaded red (primary effect on $\Delta\Delta G_c$), residues important for DNA binding are shaded blue (large effect on $\Delta\Delta G_{bind}$), while those that impact both ΔG_c and ΔG_{bind} are shaded pink/purple.

functions to effectively lower the affinity of the Cu(I)-bound state.

A particularly striking aspect of allosteric linkage in this system may be what appears to be key quaternary structural interaction between Glu73 and Lys101″ whose integrity is critical to maintaining high affinity binding in the apo-state and/or driving CsoR off the DNA in the presence of Cu(I). Since previous studies reveal that Lys101 (Lys96 in *Bsu* CsoR) is protected from amidination in *both* the Cu(I)-bound and DNA-bound states relative to the reference apo-state,[21] Lys101 is an excellent candidate for electrostatic occlusion in the Cu(I)-bound state. This is the first documentation of an functionally important dimer−dimer ion pairing interaction in any CsoR/RcnR family regulator. Finally, Arg48 is critical for CsoR DNA binding affinity *in vitro* and in cells, and either makes an energetically important contact with the DNA, or mediates an electrostatic interaction with the opposite *tetramer* in the 2:1 sandwich complex; a candidate ion-pairing partner is Asp52. Preliminary β-gal assays of *B. subtilis* strains expressing a charge reversal mutant to test the importance of a putative Arg48-Asp52 interaction reveal that all are poor repressors *in vivo* (data not shown). This suggests that Arg48 mediates a direct physical interaction with the DNA.

Although the precise path of the bound DNA across one face of the CsoR tetramer is not yet known, these data taken collectively, particularly in the context of the relative position of the RxxR motif[22] in close proximity to Arg65[15] (shaded blue or purple), and the importance of Arg48 in DNA binding, suggests that the DNA may define a path from north to south, ~30° off vertical in the orientation shown here, in which the RxxR motif and Arg48 define opposite edges of the DNA interaction site as it traverses one face of the tetramer (Figure 6). Indeed, a preliminary modeling exercise reveals that in the context of a rotationally 2-fold symmetric 2:1 sandwich complex, both the RxxR motif and Arg48 are positioned such that each is able to simultaneously interact with opposite sides of the DNA helix, near the 5′-TA|C sequence, e.g., in sites A and in Figure 2A,

DOI: 10.1021/acs.biochem.5b00154
Biochemistry 2015, 54, 2463−2472

which defines the presumed B-A helical junction.[33] This, in turn, places those more peripheral determinants of allosteric negative regulation (shaded red or pink, Figure 6) adjacent, but somewhat distant from the likely physical interface with DNA. Here, Arg74 could potentially perform both roles, weakly interacting electrostatically with the DNA in the apo-state, and undergoing occlusion upon Cu(I) binding as a result of ion pairing with Glu22. In addition, Glu73 is also distant from the proposed path of the bound DNA in this model. It is tempting to speculate, in fact, that this contiguous network of clade-specific residues (shaded yellow in Figure 1B; shaded red/pink in Figure 6) defines a physical pathway of allosteric negative linkage that mediates clade IV CsoR function. Detailed insights beyond those discussed here will require a high-resolution structure of the 2:1 apoprotein−DNA sandwich complex, which is currently being pursued in our laboratory.

■ ASSOCIATED CONTENT

Supporting Information

Supplementary Table S1 and Supplementary Figures S1−S8. These data summarize gel filtration analysis of *Gt* CsoR mutants, Cu(I)-binding data, NMR analysis of selected mutants, and species fractions simulations derived from the experiments shown in Figure 3. This material is available free of charge via the Internet at http://pubs.acs.org.

■ AUTHOR INFORMATION

Corresponding Author

*Tel: 812-856-3178. Fax: 812-856-5710. E-mail: giedroc@indiana.edu.

Author Contributions

D.P.G and F.-M.J.C. contributed to the development of the manuscript, with primary contributions from F.-M.J.C. J.E.M. constructed the *B. subtilis* strains and carried out the biological assays. This work was submitted by F.-M.J.C. to the Graduate School of Indiana University in partial fulfillment of the requirements for the Ph.D. in Chemistry.

Funding

This work was supported by NIH Grant R01 GM042569 to D.P.G.

Notes

The authors declare no competing financial interest.

■ REFERENCES

(1) Reyes-Caballero, H., Campanello, G. C., and Giedroc, D. P. (2011) Metalloregulatory proteins: metal selectivity and allosteric switching. *Biophys Chem. 156*, 103−114.

(2) Foster, A. W., Osman, D., and Robinson, N. J. (2014) Metal Preferences and Metallation. *J. Biol. Chem. 289*, 28095−28103.

(3) Ma, Z., Chandrangsu, P., Helmann, T. C., Romsang, A., Gaballa, A., and Helmann, J. D. (2014) Bacillithiol is a major buffer of the labile zinc pool in *Bacillus subtilis*. *Mol. Microbiol. 94*, 756−770.

(4) Braymer, J. J., and Giedroc, D. P. (2014) Recent developments in copper and zinc homeostasis in bacterial pathogens. *Curr. Opin. Chem. Biol. 19*, 59−66.

(5) Macomber, L., and Imlay, J. A. (2009) The iron-sulfur clusters of dehydratases are primary intracellular targets of copper toxicity. *Proc. Natl. Acad. Sci. U. S. A. 106*, 8344−8349.

(6) Fu, Y., Chang, F. M., and Giedroc, D. P. (2014) Copper transport and trafficking at the host-bacterial pathogen interface. *Acc. Chem. Res. 47*, 3605−3613.

(7) White, C., Lee, J., Kambe, T., Fritsche, K., and Petris, M. J. (2009) A role for the ATP7A copper-transporting ATPase in macrophage bactericidal activity. *J. Biol. Chem. 284*, 33949−33956.

(8) Stafford, S. L., Bokil, N. J., Achard, M. E., Kapetanovic, R., Schembri, M. A., McEwan, A. G., and Sweet, M. J. (2013) Metal ions in macrophage antimicrobial pathways: emerging roles for zinc and copper. *Biosci. Rep. 33*, No. e00049.

(9) Gourdon, P., Liu, X. Y., Skjorringe, T., Morth, J. P., Moller, L. B., Pedersen, B. P., and Nissen, P. (2011) Crystal structure of a copper-transporting PIB-type ATPase. *Nature 475*, 59−64.

(10) Gold, B., Deng, H., Bryk, R., Vargas, D., Eliezer, D., Roberts, J., Jiang, X., and Nathan, C. (2008) Identification of a copper-binding metallothionein in pathogenic mycobacteria. *Nat. Chem. Biol. 4*, 609−616.

(11) Festa, R. A., Jones, M. B., Butler-Wu, S., Sinsimer, D., Gerads, R., Bishai, W. R., Peterson, S. N., and Darwin, K. H. (2011) A novel copper-responsive regulon in *Mycobacterium tuberculosis*. *Mol. Microbiol. 79*, 133−148.

(12) Changela, A., Chen, K., Xue, Y., Holschen, J., Outten, C. E., O'Halloran, T. V., and Mondragon, A. (2003) Molecular basis of metal-ion selectivity and zeptomolar sensitivity by CueR. *Science 301*, 1383−1387.

(13) Liu, T., Ramesh, A., Ma, Z., Ward, S. K., Zhang, L., George, G. N., Talaat, A. M., Sacchettini, J. C., and Giedroc, D. P. (2007) CsoR is a novel *Mycobacterium tuberculosis* copper-sensing transcriptional regulator. *Nat. Chem. Biol. 3*, 60−68.

(14) Coyne, H. J., 3rd, and Giedroc, D. P. (2013) Backbone resonance assignments of the homotetrameric (48 kD) copper sensor CsoR from *Geobacillus thermodenitrificans* in the apo- and Cu(I)-bound states: insights into copper-mediated allostery. *Biomol. NMR Assign. 7*, 279−283.

(15) Chang, F. M., Coyne, H. J., Ramirez, C. A., Fleischmann, P. V., Fang, X., Ma, Z., Ma, D., Helmann, J. D., Garcia-de Los Santos, A., Wang, Y. X., Dann, C. E., 3rd, and Giedroc, D. P. (2014) Cu(I)-mediated allosteric switching in a copper-sensing operon repressor (CsoR). *J. Biol. Chem. 289*, 17833−17847.

(16) Dwarakanath, S., Chaplin, A. K., Hough, M. A., Rigali, S., Vijgenboom, E., and Worrall, J. A. (2012) Response to copper stress in *Streptomyces lividans* extends beyond genes under direct control of a copper-sensitive operon repressor protein (CsoR). *J. Biol. Chem. 287*, 17833−17847.

(17) Iwig, J. S., Leitch, S., Herbst, R. W., Maroney, M. J., and Chivers, P. T. (2008) Ni(II) and Co(II) sensing by *Escherichia coli* RcnR. *J. Am. Chem. Soc. 130*, 7592−7606.

(18) Foster, A. W., Patterson, C. J., Pernil, R., Hess, C. R., and Robinson, N. J. (2012) Cytosolic Ni(II) sensor in cyanobacterium: nickel detection follows nickel affinity across four families of metal sensors. *J. Biol. Chem. 287*, 12142−12151.

(19) Luebke, J. L., Shen, J., Bruce, K. E., Kehl-Fie, T. E., Peng, H., Skaar, E. P., and Giedroc, D. P. (2014) The CsoR-like sulfurtransferase repressor (CstR) is a persulfide sensor in *Staphylococcus aureus*. *Mol. Microbiol. 94*, 1343−1360.

(20) Higgins, K. A., and Giedroc, D. (2014) Insights into Protein Allostery in the CsoR/RcnR Family of Transcriptional Repressors. *Chem. Lett. 43*, 20−25.

(21) Chang, F. M., Lauber, M. A., Running, W. E., Reilly, J. P., and Giedroc, D. P. (2011) Ratiometric pulse-chase amidination mass spectrometry as a probe of biomolecular complex formation. *Anal. Chem. 83*, 9092−9099.

(22) Tan, B. G., Vijgenboom, E., and Worrall, J. A. (2014) Conformational and thermodynamic hallmarks of DNA operator site specificity in the copper sensitive operon repressor from *Streptomyces lividans*. *Nucleic Acids Res. 42*, 1326−1340.

(23) Smaldone, G. T., and Helmann, J. D. (2007) CsoR regulates the copper efflux operon *copZA* in *Bacillus subtilis*. *Microbiology 153*, 4123−4128.

(24) Fu, Y., Tsui, H. C., Bruce, K. E., Sham, L. T., Higgins, K. A., Lisher, J. P., Kazmierczak, K. M., Maroney, M. J., Dann, C. E., 3rd, Winkler, M. E., and Giedroc, D. P. (2013) A new structural paradigm in copper resistance in *Streptococcus pneumoniae*. *Nat. Chem. Biol. 9*, 177−183.

DOI: 10.1021/acs.biochem.5b00154
Biochemistry 2015, 54, 2463−2472

(25) Kuzmic, P. (1996) Program DYNAFIT for the analysis of enzyme kinetic data: application to HIV proteinase. *Anal. Biochem. 237*, 260−273.
(26) Ma, Z., Cowart, D. M., Scott, R. A., and Giedroc, D. P. (2009) Molecular insights into the metal selectivity of the copper(I)-sensing repressor CsoR from *Bacillus subtilis*. *Biochemistry 48*, 3325−3334.
(27) Xiao, Z., Donnelly, P. S., Zimmermann, M., and Wedd, A. G. (2008) Transfer of copper between bis(thiosemicarbazone) ligands and intracellular copper-binding proteins. insights into mechanisms of copper uptake and hypoxia selectivity. *Inorg. Chem. 47*, 4338−4347.
(28) Ma, Z., Cowart, D. M., Ward, B. P., Arnold, R. J., DiMarchi, R. D., Zhang, L., George, G. N., Scott, R. A., and Giedroc, D. P. (2009) Unnatural amino acid substitution as a probe of the allosteric coupling pathway in a mycobacterial Cu(I) sensor. *J. Am. Chem. Soc 131*, 18044−18045.
(29) Grossoehme, N., Kehl-Fie, T. E., Ma, Z., Adams, K. W., Cowart, D. M., Scott, R. A., Skaar, E. P., and Giedroc, D. P. (2011) Control of copper resistance and inorganic sulfur metabolism by paralogous regulators in *Staphylococcus aureus*. *J. Biol. Chem. 286*, 13522−13531.
(30) Chaplin, A. K., Tan, B. G., Vijgenboom, E., and Worrall, J. A. (2015) Copper trafficking in the CsoR regulon of Streptomyces lividans. *Metallomics 7*, 145−155.
(31) Corbett, D., Schuler, S., Glenn, S., Andrew, P. W., Cavet, J. S., and Roberts, I. S. (2011) The combined actions of the copper-responsive repressor CsoR and copper-metallochaperone CopZ modulate CopA-mediated copper efflux in the intracellular pathogen *Listeria monocytogenes*. *Mol. Microbiol. 80*, 14−21.
(32) Guerra, A. J., and Giedroc, D. P. (2014) Backbone and sterospecific methyl side chain resonance assignments of the homodimeric zinc sensor AdcR (32 kDa) in the apo- and Zn(II)-bound states. *Biomol. NMR Assign. 8*, 11−14.
(33) Iwig, J. S., and Chivers, P. T. (2009) DNA recognition and wrapping by *Escherichia coli* RcnR. *J. Mol. Biol. 393*, 514−526.

DOI: 10.1021/acs.biochem.5b00154
Biochemistry 2015, 54, 2463−2472